Geochemical Perspectives Letters

Rare evidence for the existence of a Hadean enriched mantle reservoir

V.B. Garcia, J. O'Neil, E.L. Dantas

Supplementary Information

The Supplementary Information includes:

- Methods
- Geological context
- Major and trace element compositions
- Nd isotopic compositions and disturbance
- Supplementary Figures S-1 to S-6
- Tables S-1 to S-3
- Supplementary Information References

Methods

Whole-rock geochemistry

A total of 15 amphibolite samples and two host rocks were analyzed for this study and whole-rock geochemical data is available in Table S-1. Sample preparation was conducted at the University of Ottawa. After removal of weathered surfaces, the samples were crushed using a steel jaw crusher and pulverized in an alumina shatter box. Major and trace element compositions were measured at the University of Ottawa. Major element concentrations were analyzed by X-ray fluorescence at the University of Ottawa X-ray Core Facility, using a Rigaku Supermini200 WDXRF. The glass disks were produced using a flux made in-house (79/21 $Li_2B_4O_7/LiBO_2$) and a sample:flux ratio of 1:7, with the addition of 60-80 mg of LiBr. Trace element concentrations were analyzed at the Geochemistry Core Facility of the University of Ottawa, using an Agilent 8800QQQ Triple Quadrupole ICP-MS. Powdered samples were dissolved in 4:1 mixture of $HF-HNO_3$ in Savillex Teflon beakers, dried, and re-dissolved in 6M HCl with a drop of H_3BO_3 to prevent the formation of fluorides. Standard material BHVO-2, BCR-2, BIR-1, and GSP-2 were prepared following the same procedure as the samples and measured multiple times. Precisions were <5% for the REE, Sc, Ti, V, Cr, Co, Zn, Ga, Y, Zr, Nb, Sb, Ba, Hf, Pb and <10% Ni, Cu, Ge, Sr, Ta and 15-18% for Rb, Th, U and 47% for Cs. The accuracies for repeated measurements of the BHVO-2 standard was >95% for REE, Sc, Ti, V, Co, Ni, Cu, Ga, Sr, Y, Zr, Nb, Hf, Ta, Pb, U; 90-84% for Cr, Ba, Rb, Zn, Ge, Th and 79% for Cs.

Sm-Nd isotopes

Sample preparation for isotopic analyses was conducted in the clean laboratory of the Geochemistry Core Facility at the University of Ottawa. Depending on Nd concentrations, between 20 and 150 mg of powder was dissolved for 17 samples

for measurement of their $^{147\text{-}146}$Sm-$^{143\text{-}142}$Nd isotopic compositions. Dissolution was achieved in closed Savillex Teflon beakers using the same procedure as described for trace element analyses. After dissolution, aliquots for an equivalent of 250-300 ng of Nd were taken for each sample and spiked with a ^{149}Sm-^{150}Nd mixed tracer for determination of Sm and Nd concentrations by isotopic dilution. Unspiked aliquots were used for high-precision isotopic analyses to determine ^{142}Nd/^{144}Nd and ^{143}Nd/^{144}Nd ratios.

Rare earth elements were extracted from the spiked and unspiked aliquots using primary columns filled with the same 2ml of 200-400 mesh AG50W-X8 cation exchange resin. For the spiked aliquots, Sm and Nd fractions were separated using quartz columns filled with 300 mg of 50-100 mesh Eichrom LnSpec resin. For high-precision analyses of the 142Nd/144Nd ratios, chemical separation and purification of Nd from the unspiked aliquots were achieved following the protocols of Garçon et al. (2018), and only the main steps are summarized here. After the REE extraction from the primary columns, the REE fractions were dissolved in HNO_3 with $NaBrO_3$ to oxidize Ce to its +4 form and passed through columns filled with 100-150 µm Eichrom LnSpec resin to remove Ce^{+4} from the other REE^{+3}. This procedure was performed twice to achieve almost complete Ce-removal. The Na and Br added from the $NaBrO_3$ during this step were removed using columns filled with 2ml AG50W-X8 cation exchange resin. Finally, the samples were purified from Sm and remaining Ce using extra fine 20-50 µm Eichrom LnSpec resin. The total procedural Nd blank was 16 pg.

Isotopic analyses were conducted at the Isotope Geochemistry & Geochronology Research Centre of Carleton University, Ottawa, Canada. Analyses were performed on a Thermo-Finnigan Triton thermal ionization mass spectrometer. The Sm and Nd concentrations were determined by isotopic dilution and analyses were performed using double Re filaments. Isotope ratios were measured statically in faraday cups, monitoring ^{147}Sm for mass interference corrections on Nd isotopic compositions, and monitoring ^{146}Nd and ^{155}Gd for isobaric interference corrections on Sm isotopic compositions. Each Nd run consisted of 140 ratios, while Sm runs consisted of 100 ratios, each measured with 8.39 seconds integration time per cycle. Instrumental mass bias fractionation was corrected using an exponential law and the ratios of 146Nd/144Nd = 0.7219 for Nd and ^{147}Sm/^{152}Sm = 0.56081. ^{147}Sm/^{144}Nd ratios obtained from isotopic dilution measurements of Sm and Nd concentrations are reported in Table S-3.

High-precision Nd isotopic measurements of the unspiked fractions were acquired using double zone-refined Re filaments. For each sample, ~600 ng of Nd was analyzed using a 2-step dynamic routine that provided static measurements of all Nd isotope ratios and dynamic measurements of the ^{142}Nd/^{144}Nd ratio. All measured isotopic ratios are reported in Table S-2. The masses 140 and 147 were monitored for Ce and Sm mass interference corrections. Each run consisted of 24 blocks of 25 cycles per step, for a total of 600 ratios measured, each measured with 8.39 seconds integration time and background monitoring of 30 seconds between every block. The data reduction was done offline and corrected for instrumental mass fractionation using the exponential law to ^{146}Nd/^{144}Nd = 0.7219.

High-precision isotopic measurements were conducted during 6 analytical sessions, between March 2020 and March 2023. Faraday collectors were replaced between the analytical sessions 4 and 5. ^{142}Nd isotopic compositions are reported as μ^{142}Nd values where values for individual samples are given relative to the average JNdi-1 standard value of their respective analytical session. Measurements of the JNdi-1 standard of each session are presented in Table S-2. Reproducibility on the analyses of the JNdi-1 standard for each analytical session is better than 5 ppm with a long-term average ^{142}Nd/^{144}Nd ratio of 1.141838 ± 0.000005 (2 se = 4.7 ppm, n = 51). The long-term average ratios for the JNdi-1 standard includes all analyses performed over 6 analytical sessions (n = 51). The long-term reproducibility of 4.7 ppm corresponds to the external error shown on Figures 2, 3, S-4, S-5 and S-6. The analysis of the JNdi-1 standard yielded a

long-term average $^{143}Nd/^{144}Nd$ ratio of 0.512107 ± 0.0000003 (2 sd, n = 51), within error of 0.512115 ± 0.000007 (Tanaka *et al.*, 2000).

Figure S-6 shows the $\mu^{142}Nd$ values measured in amphibolite samples against other stable Nd isotopic compositions ($\mu^{145}Nd$, $\mu^{148}Nd$, and $\mu^{150}Nd$). Despite the lower precision on other stable isotopes ratios (static measurements as opposed to $^{142}Nd/^{144}Nd$ measured via a 2-step dynamic routine), the $\mu^{145}Nd$, $\mu^{148}Nd$ and $\mu^{150}Nd$ values measured for the amphibolite and tonalite samples do not deviate from the JNdi-1 standard. No correlation between $\mu^{142}Nd$ values and other stable isotopic compositions is observed, supporting the fact that the low $^{142}Nd/^{144}Nd$ ratios measured are not the result of fractionation during analysis. Figure S-6 also includes published data obtained for samples from the Saglek-Hebron Complex (Wasilewski *et al.*, 2022) and the Pilbara craton (Murphy *et al.*, 2021), respectively showing positive $\mu^{142}Nd$ anomalies and no $\mu^{142}Nd$ anomaly. These samples were prepared using the same procedure and analyzed in the same laboratories and instrument as the Bom Jesus samples from this study. Given that 3 different sets of samples analyzed via an identical procedure and displaying negative, positive and no $\mu^{142}Nd$ anomalies, show no deviation in $\mu^{145}Nd$, $\mu^{148}Nd$, and $\mu^{150}Nd$, we conclude that the low $^{142}Nd/^{144}Nd$ ratios measured for the Bom Jesus amphibolites are inconsistent with possible fractionation during column chemistry or nuclear field shift effect, but rather result from the decay of ^{146}Sm.

Geological context

The São José do Campestre Massif extends over 6000 km^2 (Fig. S-1) and has been reworked throughout the Archean and the Proterozoic. The dominant Archean rocks are comprised in the Presidente Juscelino complex, occurring as biotite- or clinopyroxene-bearing monzogranite gneisses formed at 3.36-3.25 Ga (Dantas *et al.*, 2004). Common tonalite and amphibolite xenoliths within the Presidente Juscelino complex are typically associated with the Bom Jesus gneiss (Dantas *et al.*, 2013; De Souza *et al.*, 2007). The Presidente Juscelino also includes lenses of sillimanite-cordierite-garnet-biotite paragneisses. Additionally, the São José do Campestre Massif contains a series of juvenile Mesoarchean magmatic rocks represented by three main units: the Senador Elói de Sousa gabbro-anorthosite, the Riacho das Telhas mafic-ultramafic suite, and the Brejinho complex (Fig. S-1). The Serra Caiada greenstone belt encompasses a series of undetailed lithologies including banded iron formations, marbles, calcsilicate rocks, and associated mafic rocks.

The geochemistry and geochronology of the Bom Jesus gneiss has previously been studied by (Dantas *et al.*, 2004, 2013). These gneisses, hosting the amphibolites studied here, are banded hornblende bearing tonalite-trondhjemite-granodiorite dated at 3412 ± 8 Ma by (Dantas *et al.*, 2004, 2013). The Bom Jesus unit mainly occurs in two distinct locations named BJ-I and BJ-II. BJ-I is a finely banded gneiss (Fig. S-1), which typical geochemical composition is > 60 wt. % SiO_2, ~13 wt. % Al_2O_3, relatively high Fe_2O_3 and MgO concentrations (respectively 4-8 wt. % and 1-6 wt. %) and whole-rock Mg# ranging from 0.3 to 0.6 by (Dantas *et al.*, 2013). Incompatible trace elements concentrations are relatively high with moderately fractionated profiles with $La_{(N)}/Yb_{(N)}$ = 3-12, high $Yb_{(N)}$ = 10-15, and negative Nb-Ta anomalies. BJ-II is a tonalite gneiss (Fig. S-1) with 66-68 wt. % SiO_2, 14-15 wt. % Al_2O_3, 3-5 wt. % Fe_2O_3, 1-3 wt. % MgO, 3-4 wt. % Na_2O and K_2O/Na_2O = 0.4-0.7 with Mg# between 0.4-0.57. Incompatible trace elements also show high concentrations, but with profiles that are more fractionated than BJ-I, with $La_{(N)}/Yb_{(N)}$ = 10-59, $Yb_{(N)}$ = 4-6, and negative Nb-Ta anomalies.

Major and trace element compositions

Figure S-2, S-3, S-4, and Table S-1 show the major and trace element compositions of the Bom Jesus amphibolite xenoliths, including the migmatite-hosted xenoliths (BJ-I), tonalite-hosted xenoliths (BJ-II), and host felsic rock

samples. Major elements were recalculated to anhydrous compositions. Except for 3 migmatite-hosted samples, the Bom Jesus amphibolites are mafic in composition with SiO_2 ranging from 46.5 wt. % to 54.0 wt. %, MgO contents ranging from 7.8 wt. % to 12.7 wt. % and high Fe_2O_3 up to 17 wt. %. Migmatite-hosted BJ-I mafic xenoliths generally have more variable major element compositions compared to the more homogenous tonalite-hosted BJ-II amphibolites (Fig. S-2), with four samples displaying lower MgO and CaO, as well as high Al_2O_3 and Na_2O contents relative to other mafic amphibolite samples. The tonalitic host rocks have the high SiO_2, Al_2O_3 and Na_2O with low CaO and MgO (Fig. S-2). Although the major element compositions of a few migmatite-hosted xenoliths could suggest some extent of crustal contamination with their felsic host, the variations in incompatible trace elements such as Th, La, Nd and Ba vs. Nb (Fig. S-4) is inconsistent with crustal contamination.

All amphibolite xenoliths have high incompatible trace element concentrations with chondrite-normalized REE profiles showing variable degrees of LREE enrichment with $La_{(N)}/Yb_{(N)}$ values ranging from 2.31 to 14.34 (Fig. S-3) and relatively flat HREE, except for a few migmatite-hosted samples displaying fractionated HREE profiles. A few samples from both BJ-I and BJ-II display variable Eu anomalies. Tonalite-hosted BJ-II xenoliths show a more homogeneous REE composition with generally less pronounced LREE enrichments than migmatite-hosted BJ-I amphibolites. The highest BJ-I REE enrichment also show pronounced Nb anomalies on a primitive mantle-normalized diagram (Fig. S-3a and c). The tonalitic hosts exhibit highly fractionated REE composition (Fig. S-2f) marked by LREE enrichment and depletion in HREE. Still, their REE and HFSE concentrations are lower than the concentrations of most amphibolites (Fig. S-2e and h), which further argues against significant crustal contamination.

Later metamorphic fluids could also cause geochemical and isotopic disturbance. To assess potential element mobility, multiple trace elements were plotted against Nb, a highly immobile HFSE (Fig. S-4). Incompatible elements that have not been disturbed by fluids are expected to show correlations with Nb, whereas elements mobilized by fluids should be decoupled. The variable Th concentrations displayed by some xenolith samples (Fig. S-4a) could be the result Th mobility under upper amphibolite metamorphic conditions (Jenner *et al.*, 2009; Polat and Hofmann, 2003), which may also have produced the apparent Nb negative anomalies in the highest Th samples (Fig. S-3c). Lanthanum and Nd, contrary to Th, show better correlations with Nb, with only few samples displaying slight deviations from the general trend, suggesting a limited extent of element remobilization. However, the lack of correlations between Nd, Nb, and La with the $\mu^{142}Nd$ of the amphibolites (Fig S-4e and f) strongly suggests that element mobility had no incidence on the ^{142}Nd composition. A weaker correlation between Nb and Ba is present for most samples, with three to four main outliers from the general trend. Those outlying samples are the most likely to have the LILE significantly affected by fluid remobilization, however, they exhibit comparable $\mu^{142}Nd$ values to other, more pristine, xenoliths (Fig. S-4g). This implies that either metamorphic fluid remobilization did not affect the $\mu^{142}Nd$ composition of the xenoliths, or that the metamorphic fluids were characterized by similar $^{142}Nd/^{144}Nd$ ratios as the xenoliths, which would have no incidence on the original ^{142}Nd composition of the amphibolites.

The more variable major and trace elements of the migmatite-hosted BJ-I may also be the result of crustal reworking and not only caused by metamorphic remobilization. The BJ-I samples are often crosscut by veinlets too narrow to be removed during sample preparation, and that could have contributed to their higher SiO_2, Al_2O_3, HFSE, REE and LILE concentrations without affecting the $\mu^{142}Nd$ isotopic composition.

The apparent LREE-enrichment and Nb anomalies are also common features of subducted related rocks. One could therefore propose that a Hadean mafic crust carrying a low $^{142}Nd/^{144}Nd$ ratio, subducting during the Paleoarchean, may have imprinted its ^{142}Nd isotopic composition in the mantle source of the amphibolites. Although it is difficult to argue for or against evidence of subduction-like processes based solely on whole-rock geochemical compositions, the Bom Jesus amphibolites' geochemistry is not consistent with a convergent margin setting. Figure S-3d compares the LREE-enrichment and the extent of Nb anomalies for the Bom Jesus amphibolites to typical subduction-related and subduction-unrelated mafic rocks. The La/Nb ratio is used as a proxy for Nb anomalies because, as discussed earlier, Th may have

been more affected by element mobility. Although some migmatite-hosted samples show similar compositions to subduction-related enriched basalts in terms of Nb variation (Nb/La_{PM}) and LREE enrichment (La/Sm_{PM}), most samples, especially the tonalite-hosted samples, show geochemical compositions inconsistent with subduction-related rocks and closer to MORB and Ocean plateau basalts. Moreover, volcanic arc rocks typically display a parallel trend to the MORB-OIB array on a Th/Yb *vs*. Nb/Yb diagram (Pearce, 2008), but displaced toward higher Th/Yb ratios. Figure S-3e shows that a number Bom Jesus amphibolite samples plot above the MORB-OIB array, but displaying a trend more consistent with some extend of Th mobility rather than the volcanic arc array. The incompatible trace element compositions of the samples that appear to have not significantly been remobilized are suggestive of a mantle source more enriched than the depleted MORB mantle or the source of most Archean basalts (Fig. S-3e).

Nd isotopic compositions and disturbance

Long-lived ^{147}Sm-^{143}Nd system

All amphibolite samples have been analyzed for their long-lived ^{147}Sm-^{143}Nd isotopic composition along with their ^{142}Nd compositions. A ^{147}Sm-^{143}Nd isochron, excluding 2 clear outlying samples, yields a best-fit-line corresponding to an age of 4049.9 ± 832.8 Ma, MSWD = 290 (n = 13). This improbable age, large error and high MSWD strongly suggest that the Paleoarchean Bom Jesus amphibolites have been affected by post-magmatic processes, at least for their long-lived ^{147}Sm-^{143}Nd isotopic compositions. This is also evident from the large variation in initial $\varepsilon^{143}Nd_{(3.4\ Ga)}$ for individual samples, ranging from +3.9 to -4.1 (with 2 outlying samples $\varepsilon^{143}Nd_{(3.4\ Ga)}$ = -19.8 and -13.9). Despite evidence for some extent of open-system behavior, most Bom Jesus amphibolite exhibit $\varepsilon^{143}Nd_{(3.4\ Ga)}$ below the "normal" depleted mantle ($\varepsilon^{143}Nd_{(3.4\ Ga)}$ = ~+2.7) with an average value of +0.4 (excluding the 2 outliers). This could be consistent with a source more enriched than the depleted mantle but could also be indicative of contamination by older crust. Therefore, the data obtained for the long-lived ^{147}Sm-^{143}Nd isotopic compositions should be used with caution.

Short-lived ^{146}Sm-^{142}Nd system

As opposed to the long-lived ^{147}Sm-^{143}Nd system, the short-lived ^{146}Sm-^{142}Nd system is much less susceptible Archean events fractionating the LREE, as disturbance of the Sm/Nd ratios after the extinction of ^{146}Sm (after ~4 Ga) does not affect the $^{142}Nd/^{144}Nd$ ratios. The absence of correlation between $\mu^{142}Nd$ values and initial $\varepsilon^{143}Nd_{(3.4\ Ga)}$, Sm/Nd ratios, Nd concentrations, Nb/La ratios, or any other elements that may have been remobilized such as Th (Fig. S-4, S-5), suggests that neither the event affecting the long-lived ^{147}Sm-^{143}Nd system, nor potential element mobility or crustal contamination, have disturbed the ^{142}Nd isotopic composition. Even samples with clearly disturbed low initial $\varepsilon^{143}Nd_{(3.4\ Ga)}$, yield $\mu^{142}Nd$ values similar to the least disturbed samples (Fig. S-5f). Moreover, despite the more heterogeneous whole-rock geochemical compositions of the migmatite-hosted BJ-I amphibolites, their $\mu^{142}Nd$ values are undistinguishable from the tonalite-hosted BJ-II amphibolites (Fig. 2). This supports the fact that crustal reworking or other post-magmatic processes that may have caused the geochemical variations of the BJ-I samples, did not affect their $^{142}Nd/^{144}Nd$ ratios.

Supplementary Figures

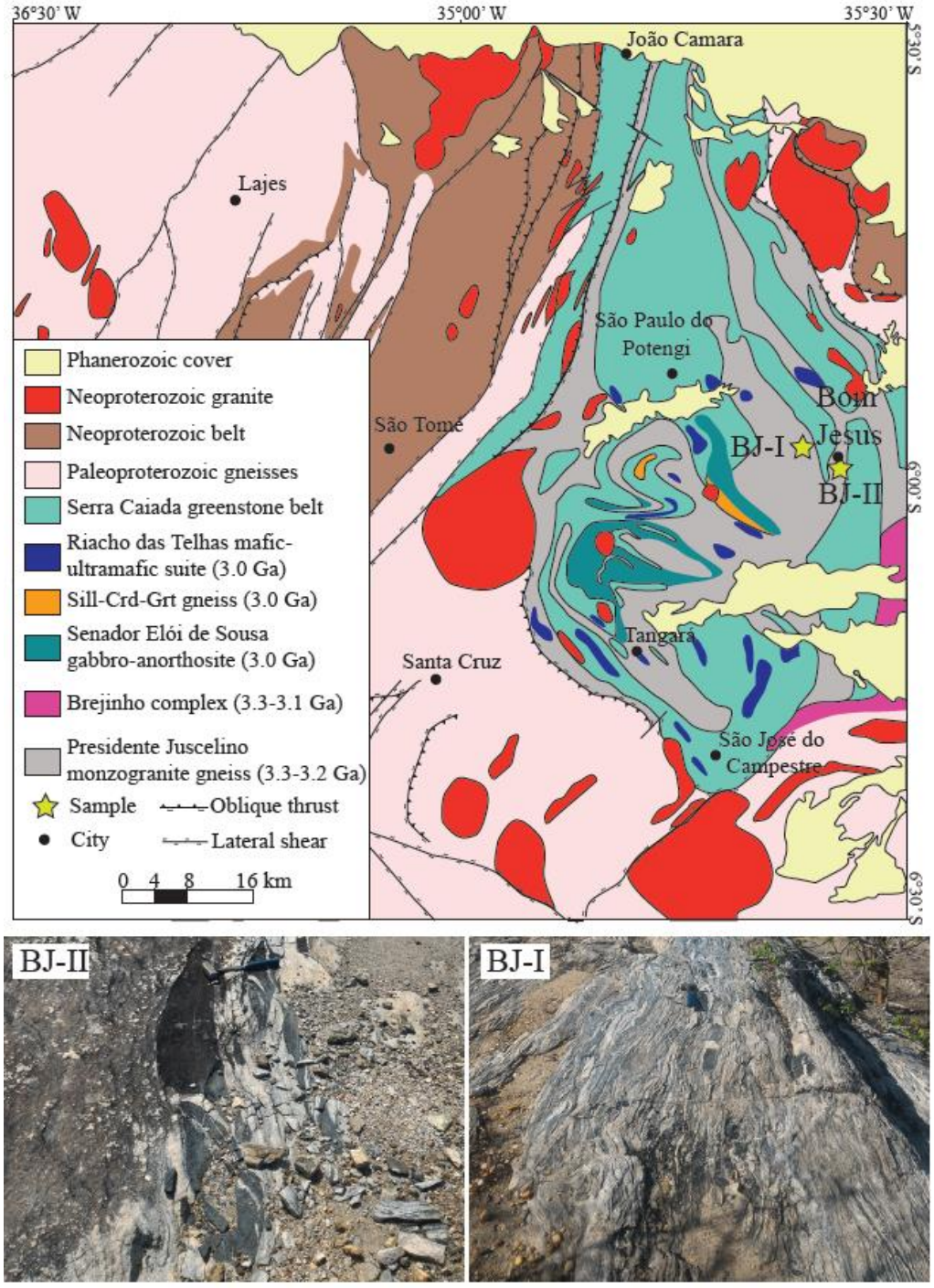

Figure S-1 Simplified geological map of the São José do Campestre massif. Locations for BJ-I and BJ-II are shown with yellow stars. Representative field photos of BJ-I and BJ-II outcrops are shown with a geological hammer for scale. The map is modified after Dantas *et al.* (2013)

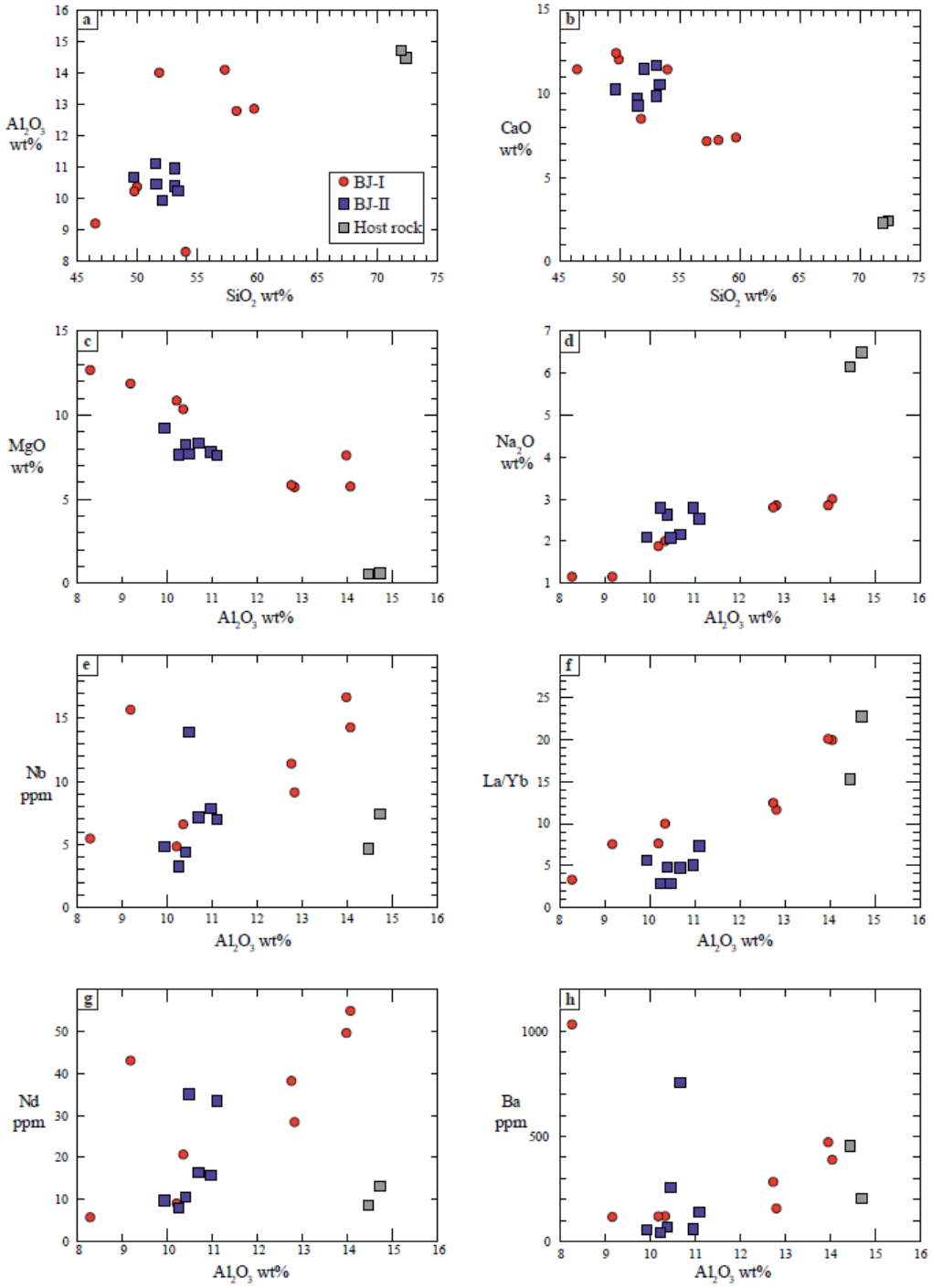

Figure S-2 Selected major element compositions vs. SiO_2 content for BJ-I, BJ-II amphibolites and host rock. Major element concentrations were recalculated to anhydrous compositions.

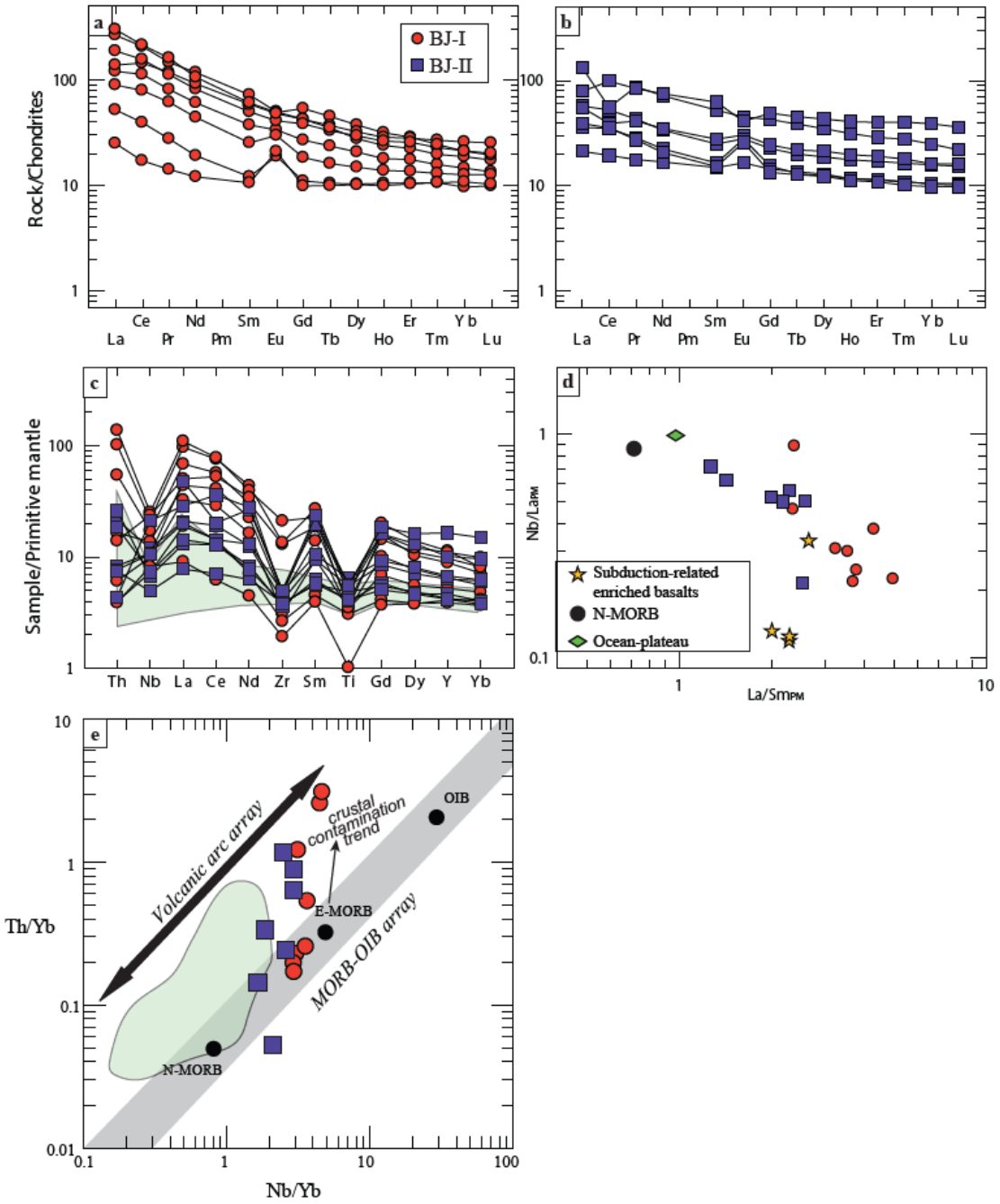

Figure S-3 Trace element compositions for BJ-I and BJ-II amphibolites. Panels **(a)** and **(b)** display chondrite-normalized REE profiles, while panel **(c)** displays multi-element patterns normalized to primitive mantle. Panel **(d)** shows the Nb/La_{PM} *vs.* La/Sm_{PM} for the Bom Jesus amphibolites compared to N-MORB and oceanic plateau (Barnes and Arndt, 2019) and subduction related enriched basalts (Jenner *et al.*, 2009). Panel **(e)** displays a Th/Yb *vs.* Nb/Yb plot after (Pearce, 2008) showing the composition of the Bom Jesus amphibolites compared to the volcanic arc and MORB-OIB arrays. The shaded field in **(c)** and **(e)** represent common Archean basalts.

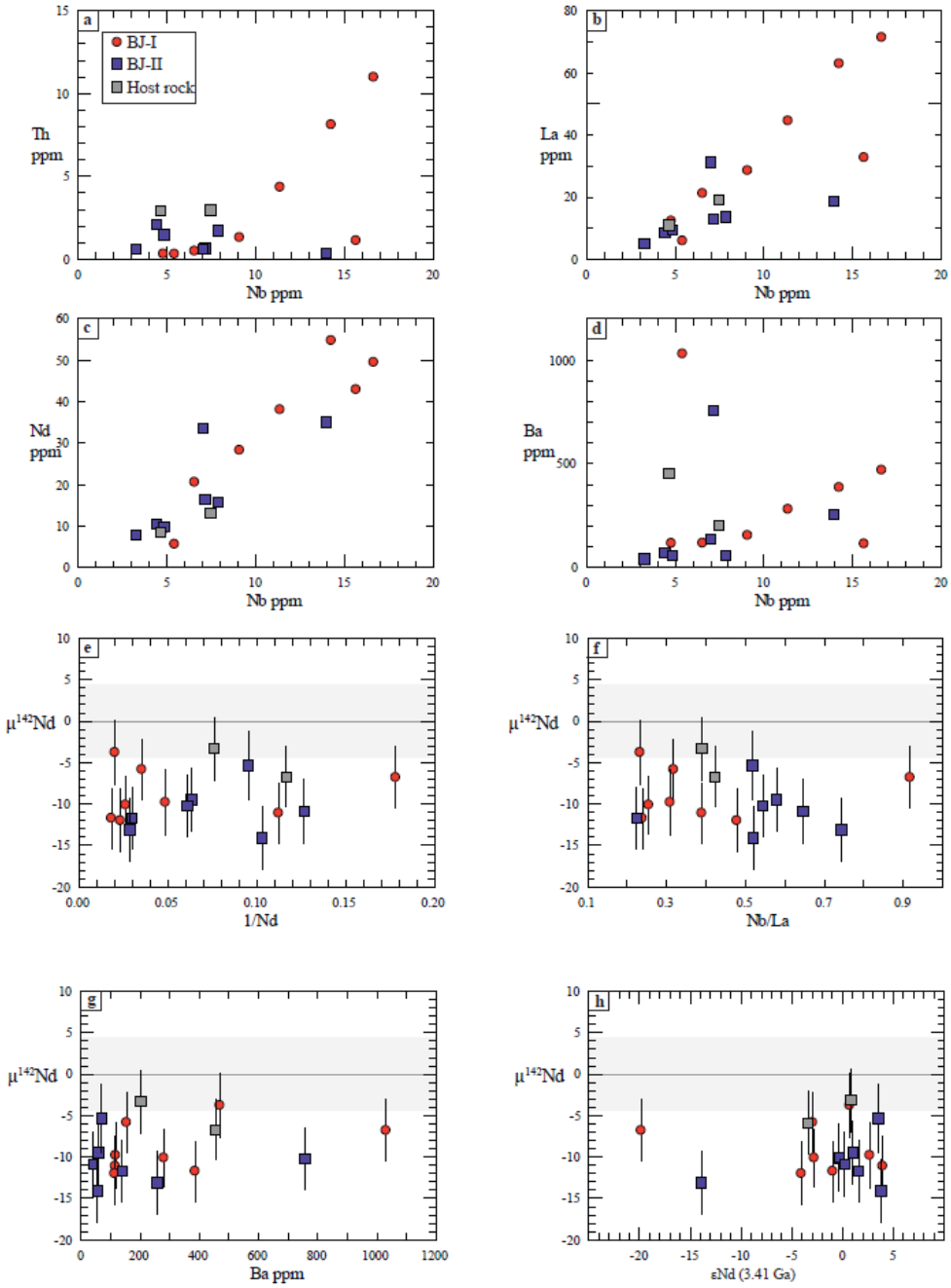

Figure S-4 Various isotopic and trace element plots for the Bom Jesus amphibolites. Panel **(a)** shows a lack of Th correlation with Nb as the result of remobilization during metamorphism. Panels **(b)** and **(c)** show the correlation of La and Nd with Nb for all samples, suggesting that possible remobilization had a limited effect on LREE. Panels **(d)** correlates Ba and Nb with a few samples outlying from the general trend suggesting a LILE metamorphic remobilization. Panels **(e-h)** highlight the lack of correlation between $\mu^{142}Nd$ and Nd concentration, Nb anomaly, Ba and $\varepsilon Nd_{(3.4Ga)}$ suggesting that the $^{142}Nd/^{144}Nd$ ratios measured in the mafic xenoliths are not changed by post-magmatic disturbance that perturbed the long-lived ^{147}Sm-^{143}Nd system. The horizontal grey bar at $\mu^{142}Nd = 0$ the external error of ± 4.7 ppm on the JNdi-1 standard.

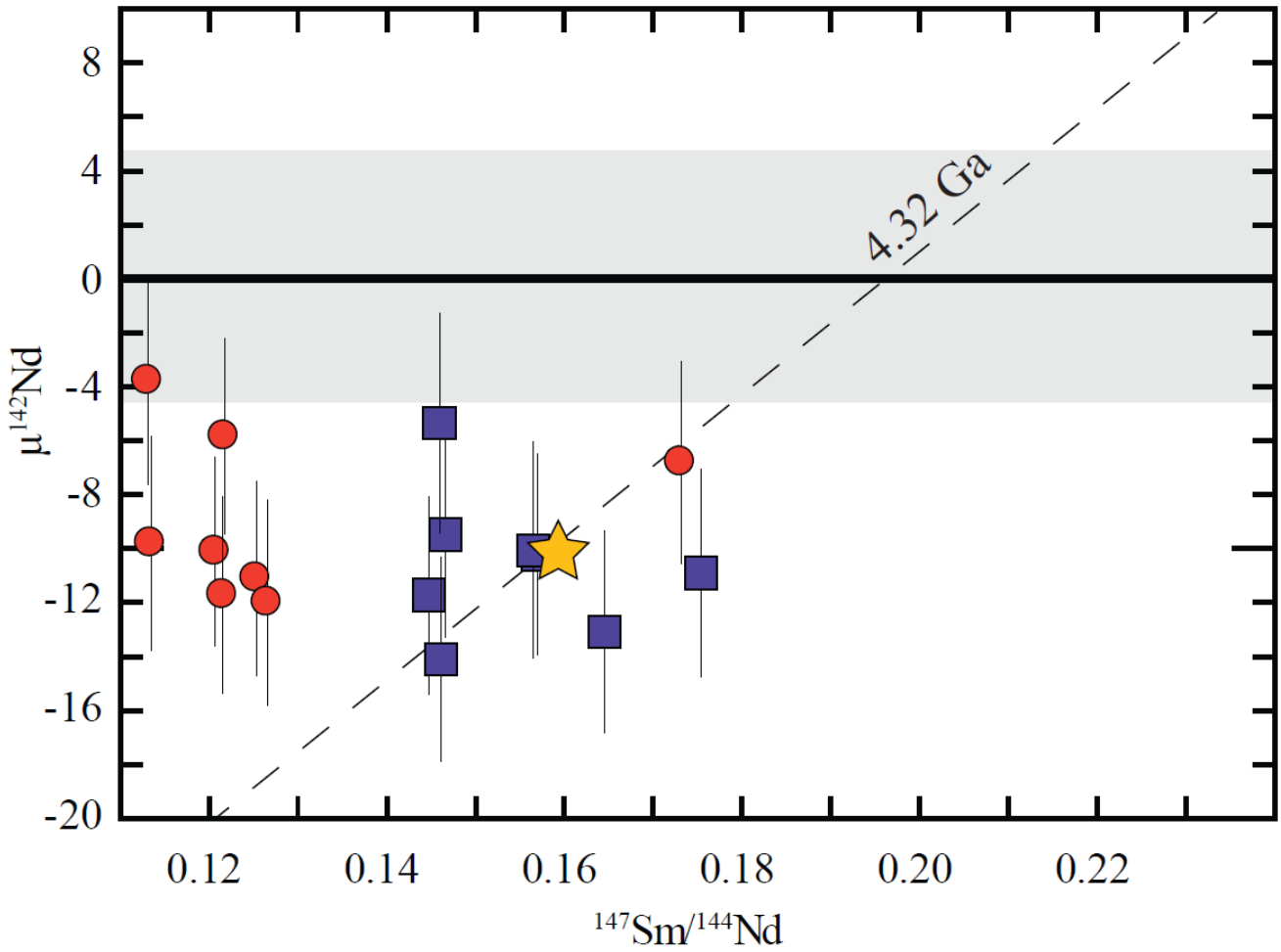

Figure S-5 $\mu^{142}Nd$ *vs.* $^{147}Sm/^{144}Nd$ plot for the Bom Jesus amphibolites. The horizontal grey band represents the external error of ±4.7 ppm on the JNdi-1 standard ($\mu^{142}Nd = 0$). The dashed line illustrates the correlation expected for a mafic crust formed at 4.32 Ga, derived from a reservoir with chondritic $^{147}Sm/^{144}Nd$ and present-day $^{142}Nd/^{144}Nd$ corresponding to the modern terrestrial mantle. It passes through the average $^{147}Sm/^{144}Nd$ ratio of 0.142 and average $\mu^{142}Nd$ value of -10.2, obtained for BJ-I and BJ-II samples (star symbol). The lack of correlation shown by the Bom Jesus amphibolites is inconsistent with a Hadean age. However, a post-crystallization disturbance may have affected the $^{147}Sm/^{144}Nd$ ratios of the amphibolites without affecting their $^{142}Nd/^{144}Nd$, which would obscure such correlation. Red circle: BJ-I; Blue square: BJ-II.

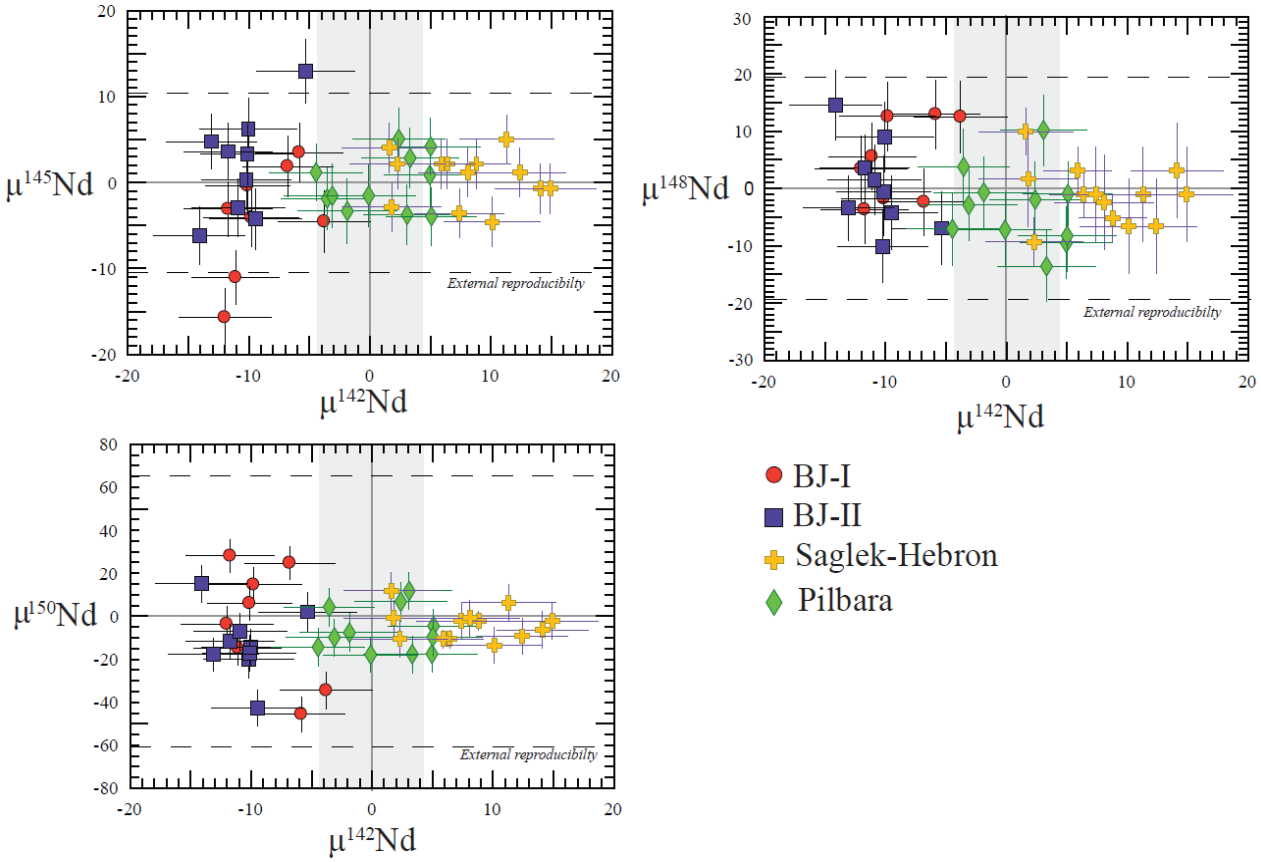

Figure S-6 μ^{145}Nd, μ^{148}Nd and μ^{150}Nd values vs. μ^{142}Nd values for the Bom Jesus amphibolites. ^{142}Nd/^{144}Nd ratios were measured in a 2-step dynamic routine, while ^{145}Nd/^{144}Nd, ^{148}Nd/^{144}Nd and ^{150}Nd/^{144}Nd ratios were measured statically. Grey bands show the external error on μ^{142}Nd of 4.7 ppm obtained from repeated measurements of the JNdi-1 standard while the dashed lines show the external errors on the μ^{145}Nd, μ^{148}Nd, and μ^{150}Nd values. Data from the Saglek-Hebron Complex and Pilbara craton are from (Wasilewski *et al.*, 2022) and (Murphy *et al.*, 2021) and analyzed in the same laboratories as the Bom Jesus samples, using the same procedure and instrument.

Supplementary Tables

Table S-1 Major (wt. %) and trace (ppm) element concentrations for the Bom Jesus amphibolites and host rock (.xlsx)

Table S-2 High precision Nd isotope measurements for the JNdi-1 Nd standard and the Bom Jesus samples. Errors on individual measurements are 2 SE, and errors on averages are 2SD (.xlsx)

Table S-3 Sm-Nd and ^{142}Nd/^{144}Nd isotopic data for the Bom Jesus amphibolites and host rock. (.xlsx)

Table S-1 to S-3 (.xlsx) are available for download from the online version of this article at https://doi.org/10.7185/geochemlet.2336

Supplementary Information References

Barnes, S.J., Arndt, N.T. (2019) Distribution and Geochemistry of Komatiites and Basalts Through the Archean. In: Van Kranendonk, M.J., Bennett, V.C., Hoffmann, J.E. (Eds.) *Earth's Oldest Rocks*, 103–132.

Dantas, E.L., De Souza, Z.S., Wernick, E., Hackspacher, P.C., Martin, H., Xiaodong, D., Li, J.W. (2013) Crustal growth in the 3.4-2.7Ga São José de Campestre Massif, Borborema Province, NE Brazil. *Precambrian Research* 227, 120–156, https://doi.org/10.1016/j.precamres.2012.08.006.

Dantas, E.L., Van Schmus, W.R., Hackspacher, P.C., Fetter, A.H., De Brito Neves, B.B., Cordani, U., Nutman, A.P., Williams, I.S. (2004) The 3.4-3.5 Ga São José do Campestre massif, NE Brazil: Remnants of the oldest crust in South America. *Precambrian Research* 130, 113–137, https://doi.org/10.1016/j.precamres.2003.11.002.

De Souza, Z.S., Martin, H., Peucat, J.J., Jardim De Sá, E.F., De Freitas Macedo, M.H. (2007) Calc-alkaline magmatism at the Archean-Proterozoic transition: The Caicó Complex Basement (NE Brazil). *Journal of Petrology* 48, 2149–2185, https://doi.org/10.1093/petrology/egm055.

Garçon, M., Boyet, M., Carlson, R.W., Horan, M.F., Auclair, D., Mock, T.D. (2018) Factors influencing the precision and accuracy of Nd isotope measurements by thermal ionization mass spectrometry. *Chemical Geology* 476, 493–514, https://doi.org/10.1016/j.chemgeo.2017.12.003.

Jenner, F.E., Bennett, V.C., Nutman, A.P., Friend, C.R.L., Norman, M.D., Yaxley, G. (2009) Evidence for subduction at 3.8 Ga: Geochemistry of arc-like metabasalts from the southern edge of the Isua Supracrustal Belt. *Chemical Geology* 261, 83–98, https://doi.org/10.1016/j.chemgeo.2008.09.016.

Murphy, D., Rizo, H., O'Neil, J., Hepple, R., Wiemer, D., Kemp, A., Vervoort, J. (2021) Combined Sm-Nd, Lu-Hf, and ^{142}Nd study of Paleoarchean basalts from the East Pilbara Terrane, Western Australia. *Chemical Geology* 578, 120301, https://doi.org/10.1016/j.chemgeo.2021.120301.

Pearce, J.A. (2008) Geochemical fingerprinting of oceanic basalts with applications to ophiolite classification and the search for Archean oceanic crust. *Lithos* 100, 14–48, https://doi.org/10.1016/j.lithos.2007.06.016.

Polat, A., Hofmann, A.W. (2003) Alteration and geochemical patterns in the 3.7-3.8 Ga Isua greenstone belt, West Greenland. *Precambrian Research* 126, 197–218, https://doi.org/10.1016/S0301-9268(03)00095-0.

Tanaka, T., Togashi, S., Kamioka, H., Amakawa, H., Kagami, H., Hamamoto, T., Yuhara, M., Orihashi, Y., Yoneda, S., Shimizu, H., Kunimaru, T. (2000) JNdi-1: A neodymium isotopic reference in consistency with LaJolla neodymium. *Chemical Geology* 168, 279–281, https://doi.org/10.1016/S0009-2541(00)00198-4.

Wasilewski, B., O'Neil, J., Rizo, H. (2022) Archean crustal evolution of the Saglek-Hebron Complex, Northern Labrador, revealed from coupled 147−146Sm-143−142Nd systematics. *Earth and Planetary Science Letters* 594, 117735, https://doi.org/10.1016/j.epsl.2022.117735.